Engineering Structures 178 (2019) 12–23

Contents lists available at ScienceDirect

Engineering Structures

journal homepage: www.elsevier.com/locate/engstruct

Large-scale test as the basis of investigating the fire-resistance of underground RC substructures

Limin Lu[a], Junnan Qiu[b], Yong Yuan[c,*], Jin Tao[d], Haitao Yu[a,c], Hui Wang[c,e], Herbert Mang[c,e]

[a] State Key Laboratory for Geomechanics and Deep Underground Engineering, China University of Mining and Technology, Xuzhou, China
[b] Shanghai SMI Highway Group, CO. LTD, Shanghai, China
[c] State Key Laboratory of Disaster Reduction in Civil Engineering, Tongji University, Shanghai, China
[d] Civil Engineering School, Southeast University, Nanjing, China
[e] Institute for Mechanics of Materials and Structures, Vienna University of Technology, Vienna, Austria

ARTICLE INFO

Keywords:
Underground structures
Reinforced concrete frame
Fire test
Structural fire performance
Spalling

ABSTRACT

Fire disasters occurring in underground structures generally result in severe damage. In order to investigate the fire performance of typical underground structures, a large-scale fire test on a three-span frame structure was carried out. The tested model was loaded both by vertical and horizontal earth pressures. The applied temperature history, representing the time-dependent fire load, was determined by simulations of fire scenarios in the underground structure with the help of the software FDS. The paper contains test results of the temperature of the air in the furnace, the concrete and the steel bars in the structural model, and the state of deformation of the model. Apparent phenomena, such as cracking and spalling, were observed throughout the whole testing process. The results show that a very dangerous situation of the underground structure exposed to fire may occur during the cooling process. Curling of the top slab was observed during the heating process. More attention in fire-resistance design must be paid to the columns. The fire test results are useful for validation of numerical models and for further fire-resistance research of underground structures.

1. Introduction

Fire disasters in underground structures have generally resulted in severe damage of structures [17,5,10,30]. As indicated by performance-based fire resistance design, research results for ground structures cannot directly be used for underground structures, because of different fire scenarios and of different restraint conditions and loads [4,9,7,2].

During the last decades, a large number of simulations of structures subjected to fire, using the Finite Element Method (FEM), were reported in the literature [13,18]. In particular, fire scenarios, i.e. temperature fields to which the underground structures were assumed to be subjected and their performance under the resulting temperature loads, were thoroughly investigated. Savov et al. [22] have studied the behavior of shallow tunnels, subjected to fire loads, by simulating the structure with the "beam-spring" model. Concrete spalling of the tunnel lining was simulated and its influence on the collapse of the structure was analyzed, considering the failure mechanism of beams, modeled by the FEM. This permitted prediction of the failure mode of the tunnel structure. Ring et al. [19] have simulated the behavior of underground tunnels subjected to various fire scenarios, considering different material parameters and structural models. They have performed research of the spalling problem and on the effect of load-induced thermal strains (LITS). Amouzandeh [1] has carried out a series of FE simulations, including treatment of the burning process of fire in tunnels by means of CFD (Computational Fluid Dynamics) and analyses of the structural performance. Their calculations and analyses revealed that the fire resistance of the tunnel with a circular cross-section is greater than the one of tunnels with a rectangular cross-section. Zeiml et al. [29] have investigated the safety of an underground frame structure subjected to fire, with the help of the FEM.

Due to the complexity of fire tests and the constraints of the test facilities, the number of large-scale fire tests is relatively small. Most of such tests on underground structures refer to tunnels. Yan et al. [25,26] carried out full-scale experiments to investigate the damage of the lining of a reinforced concrete (RC) metro shield TBM tunnel subjected to the standard ISO834 fire curve. Yasuda et al. [28] conducted full-scale tests on composite segments of a shield tunnel, with different methods of fire protection, subjected to a fire according to the standard RABT fire curve, which was assumed as the temperature history of tunnel fires. Spalling of concrete was observed during the experiment,

* Corresponding author.
E-mail address: yuany@tongji.edu.cn (Y. Yuan).

https://doi.org/10.1016/j.engstruct.2018.09.083
Received 18 May 2018; Received in revised form 24 August 2018; Accepted 28 September 2018
0141-0296/ © 2018 Elsevier Ltd. All rights reserved.

as deep as 60 mm in case of no fire protection on the surface. These fire tests were all based on standard fire curves, which may not allow realistic simulations of a real fire. Thus, such tests may not reveal the real structural performance.

As for underground frame structures, only few research results were reported in the literature. Park et al. [17] have performed a series of in situ investigations on the Daegu station, South Korea, which was damaged in a fire, in 2003. The damage degree of concrete was recorded and evaluated in detail. Jiang et al. [8] have carried out a series of in-situ tests of a concrete culvert. Based on these tests, they proposed a procedure for repair. Li et al. [10] reported on the repair of a frame in a structural underground passage, which suffered from a severe fire disaster, based on the results from an in-situ investigation. The structural properties before and after the repair were compared and analyzed. Annerel et al. [3] carried out five tests on slab-column substructures in order to investigate the influence of the fire load on the punching shear resistance of the slab-column connection. The test results have shown that the column and the slab-column joint experience an increased amount of spalling, which greatly increases the danger of punching shear failure of the structure. Ring et al. [21,20] have performed fire tests on four large-scale RC frame structures. The fire load was based on the standard RABT fire curve. After the tests, they analyzed the structural performance with different numerical models. However, only vertical earth pressure of the underground structures was considered, which does not represent the real loading of underground structures. The literature review has shown that the structural performance of underground frame structures, subjected to fire tests on the structural level, was often not thoroughly investigated. Thus, in order to better understand the behavior of underground structures, subjected to complex combinations of mechanical and fire loads, further research is necessary.

Full-scale fire tests are expensive and difficult to realize. This has motivated the development of the theory of scaled fire tests. McGuire et al. [12] have proposed a theory of heat conduction in scaled tests, and they have developed a design method, based on changing the time of fire exposition instead of changing the temperature field. An empirical time-scale coefficient was suggested and validated by a series of small scaled tests. O'Connor and Silcock [14] have proposed a complete design system of scaled tests based on the results of McGuire. The results corroborated the theoretical research of scaled tests. They have shown that, due to the “membrane effect”, the temperature field of the scaled models is lower than expected. In order to solve this problem, O'Connor et al. [15,16] and his team proposed a design method, which was then verified by experimental results. However, this method has some limitations: (1) the temperature curve of the air needs to be adjusted to be consistent with the test; (2) the temperature gradient is greater in the scaled tests than in reality; (3) the scaled tests and the resulting theory are not applicable to investigate the process of spalling; (4) since the temperature curve for the fire of the scaled test must increase sharply in the early phase, the requirements for the heating equipment are very high. They cannot be met even if the scale factor is greater than it should actually be. According to the literature review, there is no generally accepted theory for scaled fire tests and, consequently, no technology for scaled fire tests of reinforced concrete members. Most of the scaled tests were carried out on scaled models of real fire scenarios, which have proved to be acceptable.

In this paper, a comprehensive experimental study on the structural performance of a large-scale substructure of an underground subway station, simultaneously subjected to bidirectional loading and fire, is presented. The test procedure, the measurement systems and correspond test results were illustrated and discussed, after which conclusions for fire performance of large-scale specimen were proposed.

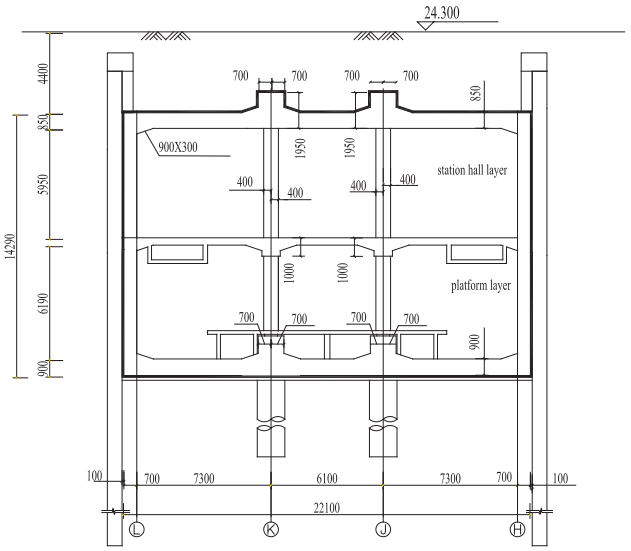

Fig. 1. Cross-section of a typical subway station.

2. A typical underground station and typical fire scenarios

2.1. Topography

The underground structure investigated in this project is a typical subway station. It consists of a two-story three-span RC structure, as shown in Fig. 1. The internal span of the selected subway station is 20.7 m with two columns in between. The size of the columns is 1.2 m × 0.8 m. The internal height of the station hall layer, i.e. the upper story of the underground station in Fig. 1, is 5.95 m and that of the platform layer, i.e. the lower story of the underground station in Fig. 1, is 6.19 m. The substructure, investigated in the fire test, is a large-scale model of the station hall layer, which is a one-layer, three-span RC frame. As regards the station hall layer, the thickness of the top slab is 0.85 m, the one of the bottom slab is 0.9 m, and the one of the lateral wall is 0.7 m.

2.2. Vertical and horizontal earth pressures

At first, the mechanical loading, acting on the subway station, i.e. the vertical and the horizontal earth pressure, are determined in order to study the structural performance. The depth from the ground surface to the top slab of the underground subway station is set as 3.5 m. According to the building codes *Standard for Metro design* [24] and *Eurocode 2* [6], the vertical and the horizontal earth pressure, representing the main action on the subway station, are determined on the basis of the following regulations:

(1) According to the load standards, the effective traffic load on the ground is 20 kN/m.
(2) The pedestrian load on the station hall layer and the platform layer is given as 4 kN/m.
(3) The thickness of the earth layer on top of the structure is given as 3.5 m, and the specific gravity of the soil is 19 kN/m^3. The average coefficient of the earth pressure at rest is chosen as 0.3.
(4) The ground water level is assumed as 0.5 m and the specific gravity of water is 9.8 kN/m^3. The water pressure and the earth pressure are calculated separately.

The load combination factor for dead load is 1.35 and that for live load is 1.4. The total combined loads for the two-layer station are shown in Table1.

Table 1
Loads acting on the subway station.

	Water pressure (kN)	Earth pressure (kN)	Live load (kN)	Combined load (kN)
Top slab	28.42	55.18	20	140.86
Top of the wall	28.42	36.4188	13.2	106
Bottom of the wall	168.462	117.5882	13.2	404.6
Bottom slab	168.462			227.4

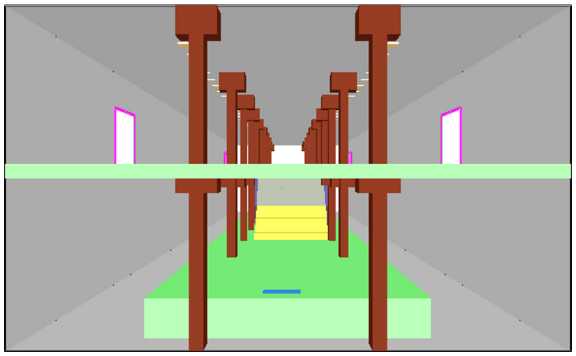

Fig. 2. Model of the investigated subway station (perspective drawing obtained from FDS).

2.3. Simulations of the most unfavorable fire scenario

Firstly, fire scenarios in underground structures are studied in order to be able to investigate the structural performance in case of fire disasters. The typical "two layers, two columns" subway station, as shown in Fig. 2, is modeled on the basis of the actual topography, as illustrated in Fig. 1, by FDS [11], which is widely used in fire simulations.

The simulated fire scenarios are designed based on the frequency and the potential damage of fire accidents. Determination of these scenarios makes use of the following information:

(1) The mechanical ventilation and the automatic sprinkler devices are considered. There are outlets every 3 m on both sides of the platform layer. The ventilation velocity is set as 2.5 m/s according to the code.
(2) The heat release rate of the fire in the subway station is 5 MW [27].
(3) The fire source is assumed to be in the middle of the platform layer, in the middle of the station hall layer, and on the train, respectively.
(4) The simulation time is set as 120 mins, which is the same as the minimum requirement of the fire resistance time for underground structures, proposed by the *Standard for Metro Design* [24].

According to the simulation results from different fire scenarios, the highest temperature of the air was obtained by assuming the fire source in the middle of the platform layer. This was regarded as the most unfavorable fire scenario. The corresponding time-dependent temperature curve, see Fig. 3, was taken as the fire curve for the fire test.

3. Test setup

3.1. Scaled model of the substructure

A model of the substructure of the station hall layer of the subway station in Fig. 1 was investigated. The tested model represents the substructure at the reduced scale of 1:4, considering the dimensions of the furnace. Defining $C = 1/4$ as the geometric scale factor, the ratios for N dimensional parameters is C^n.

(1) The width of the model was 5.26 m. Its height was 1.88 m. Limited by the dimensions of the furnace and the laboratory, the length of the model was 1.2 m.

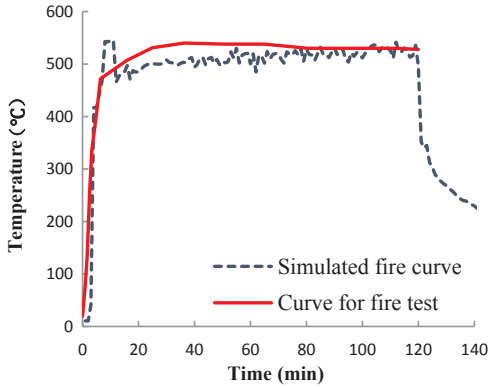

Fig. 3. Simulated temperature curve for the investigated subway station.

(2) The dimensions of the top slab and of the walls of the substructure were calculated on the basis of the scale factor, equal to one fourth of the corresponding actual dimensions of the station hall layer.
(3) The dimensions of the columns and of the bottom slab of the model were determined on the basis of the equivalent stiffness principle. The columns in the station mainly take the vertical loads while barely carrying bending moments. Therefore, the equivalent compressive stiffness, K, calculated by Eq. (1), was considered to be the key factor for determining the size of the columns,

$$K = \frac{EA}{L} \tag{1}$$

where E and A denote the elastic modulus and the cross-sectional area of the column, respectively, and L is the length of the investigated substructure.

Since the material properties and the reinforcement ratio of the tested model were chosen to be the same as for the structure, their elastic moduli are the same. The distance between the columns in the longitudinal direction of the subway station is 7.5 m. Thus, it should be 1.875 m in the model, considering the scale factor $C = 1/4$. However, the length of the model was set as 1.2 m, because of space limitations of the testing facilities. The original dimensions of the columns in the subway station are 1.2 m × 0.8 m, whereas the dimensions in the model are 0.24 m × 0.16 m, considering the scale factor $C = 1/4$ and the equivalent compressive rigidity, i.e.

$$K = \frac{E(1.2 \times C)(0.8 \times C)}{1.875} = \frac{E(0.24 \times 0.16)}{1.2} \tag{2}$$

(4) The influence of the platform layer on the stiffness of the station hall layer is accounted for by adjusting the thickness of the bottom slab of the substructure considered. By setting the thickness equal to 0.76 m, the values of the inner forces of the substructure are close to those of the whole structure, subjected to the mechanical loading. Since the scale factor is $C = 1/4$, the thickness of the bottom slab of the model is 0.19 m. The geometric dimensions of the model are shown in Fig. 4.

The reinforcement ratio of the tested model is the same as the one of the real structure. The type of the steel bars is HRB 400, and the thickness of the concrete cover is 30 mm.

(1) The reinforcement of the top slab is ⌀14@120 for the top and bottom layers in the cross-section and ⌀12@150 for the top and bottom layers in the direction perpendicular to the cross-section.
(2) The reinforcement of the bottom slab is ⌀12@100 for the layers in the cross-section and ⌀10@150 for the ones perpendicular to it.
(3) The reinforcement of the walls is ⌀14@100 for the layers in the

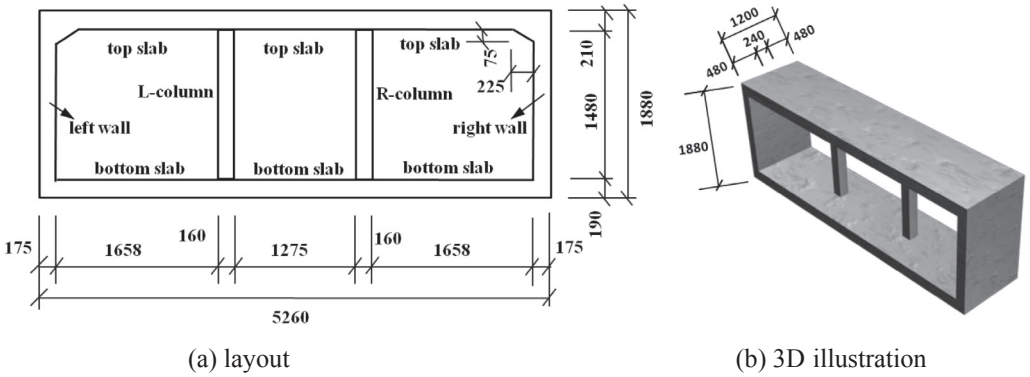

Fig. 4. Geometric dimensions of the tested structure (mm).

cross-section and ⌀10@150 for the ones perpendicular to the cross-section.

For all the slabs and walls, the stirrups are chosen as ⌀6@150 × 200 for the vicinity at the ends of the members and as ⌀6@300 × 200 for the middle part of the members, as shown in Fig. 5.

(4) The reinforcement in the columns is ten bars of ⌀12, as shown in Fig. 5.

3.2. Material properties

The concrete used for the tested model is normal concrete. Table 2 contains details of the concrete mix.

Material tests were conducted on the concrete samples, produced together with the RC frame model, in order to obtain the material properties before and after the large-scale fire test. The material tests were carried out according to the requirements by the *Standard of Testing of Mechanical Properties of Ordinary Concrete* [23]. The average value of the elastic modulus of concrete at room temperature is 2.57×10^4 MPa and the average value of the compressive strength is 36.5 MPa.

The steel bars used in the model of the RC frame were HRB 400 ⌀12 and ⌀14. Both the strength and the elastic modulus of these two types

Table 2
Mix of the employed concrete.

Mix	Content (kg/m^3)
Cement (42.5 PO)	249
Water (normal)	176
Sand 1 (middle size)	306
Sand 2 (middle size)	458
Grave stone (5–25 mm)	1013
Fly ash (Level II)	70
Additive (ZK 904-3)	6.01
Mineral powder (S95)	95

Table 3
Material properties of the steel bars.

Diameter	Yield stress (MPa)	Ultimate strength (MPa)	Elastic modulus (MPa)
12	531.9	646.4	19.3×10^4
14	530.2	666.3	19.7×10^4

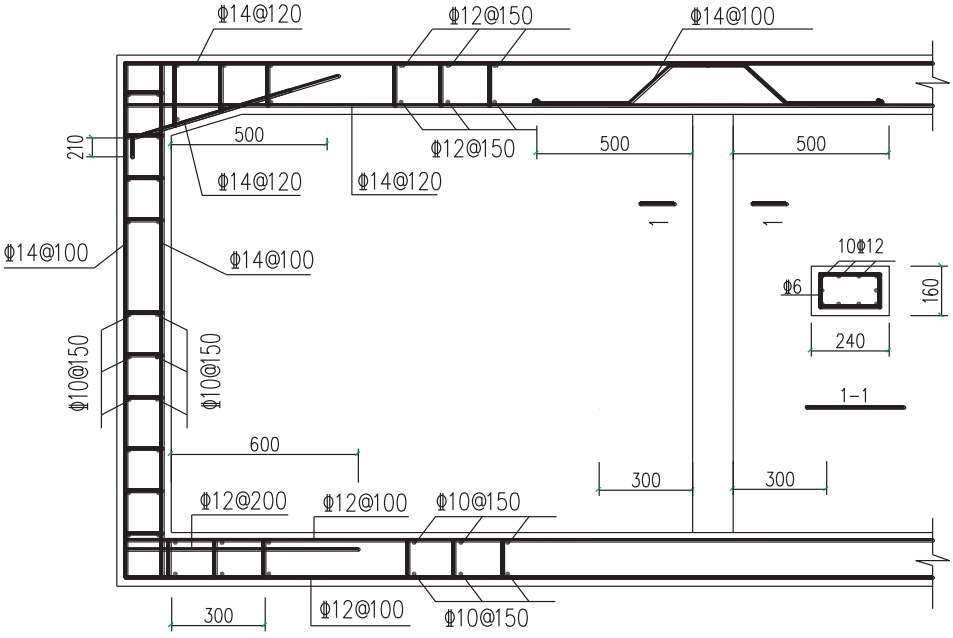

Fig. 5. Reinforcement of the tested structure (mm).

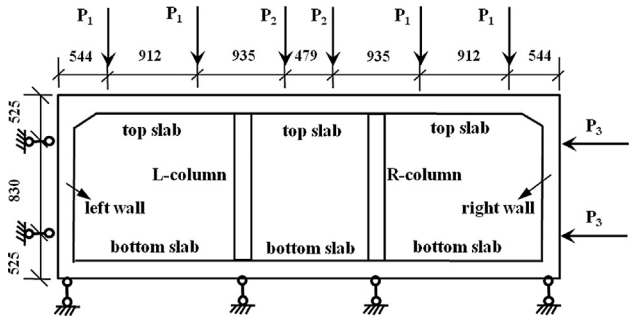

Fig. 6. Loading system.

of steel bars were tested with 8 specimens. Average values of the strength and of the elastic modulus are listed in Table 3.

3.3. Test procedure

The fire test consists of three steps: (1) proportional loading of the vertical and the horizontal earth pressures at room temperature, (2) thermal loading according to the time-dependent temperature history, and (3) removal of the thermal loading. The mechanical loads are kept constant during the last two steps.

The aim of the first step is to simulate the mechanical state of the subway station at service conditions. The actual distribution of the pressure loads is rather complicated. Therefore, the external pressures are replaced by three sets of point loads, P_1, P_2, and P_3, see Fig. 6. The resulting internal stresses are mechanically similar to the ones resulting from the real pressure distribution in the model. The values of the three sets of point loads are listed in Table 4.

The test setup is illustrated in Fig. 7. The model of the substructure was placed sidelong on the top of the furnace. The load acting on the top slab simulates the vertical earth pressure. It was applied by three hydraulic jacks acting at six load points, and the reactions were carried by four hinge supports on the bottom slab. The load acting on the lateral slab simulates the horizontal earth pressure. It was applied by one hydraulic jack acting at two load points on the right wall, while the reactions were carried by two hinge supports on the left wall, see also Fig. 6. During heating, the top of the model was covered. The data acquisition system recorded the test results. The bottom slab of the model was protected by a fire-resistant cotton as is the case in real fire conditions of underground stations.

After setup of the RC frame in the furnace and check of the whole equipment and of the functioning of the measurement devices, the loading process was started. It lasted half an hour. The hydraulic jacks were monitored such that the load was applied in the form of nine steps until the designed load was reached, see Table 4. During this process, the displacements and the strains of the steel bars were recorded.

After termination of the mechanical loading process, the fire disaster was simulated without changing the mechanical loading. The fire load, which was described in Section 2.3, was applied. The fire lasted for 2 h. The temperature in the furnace and the one of the members, their displacements, and the strains of steel bars were recorded during this process.

The third process consisted of simulating the cooling procedure within the framework of a fire disaster in underground structures. During this process the mechanical loading stayed the same. The fire was stopped and, consequently, the temperature of the air in the furnace was decreasing. This lasted for half an hour. During this process, the temperature inside the furnace, the one of the concrete and of the steel bars, the strains of the steel bars, the displacements of the structure, and the amount of spalling of the concrete cover were measured.

Thereafter, the loading system was removed from the structure.

Table 4
Mechanical loads applied to the structure.

P_1 (kN)	P_2 (kN)	P_3 (kN)
192.0	151.2	120.0

3.4. Measurements

3.4.1. Measurement of temperature

The temperature fields of the furnace and of the structure are critical parameters in the fire test. The temperature of the air in the furnace and the one of the concrete and the steel bars of the model were measured. The furnace was heated by 8 burner nozzles, placed symmetrically with respect to the longitudinal axis, to achieve a uniform temperature field. Thermal couples used to record the air temperature in the furnace were also placed symmetrically with respect to the longitudinal axis in the middle of each span of the top slab, to allow for a comparison of measurement results. Considering the complexity of the fire tests, at least two groups of thermal couples were arranged to ensure the integrity of the measured data.

Based on the described measurement concept, three K-type thermocouples were placed close to the inner surface of the top slab in order to record the air temperature inside the furnace. They are designated as TA37, TA38 and TA39, see Fig. 8.

In order to measure the temperature of the concrete, several groups of thermal couples were installed at different locations of the structure. There are either five or seven thermal couples in each group. They are distributed equally along the thickness of the monitored plate.

(1) There are six monitored locations on the top slab, and in total there are 28 couples along the depth of the slab, designated as TC1 to TC28, as shown in Fig. 9. A designation such as “5a” means that there are five thermal couples at this location along the thickness of the slab.
(2) The temperature of the bottom slab is not expected to change significantly as it is covered by a fire-resistant surface. One thermal couple, designated as TC34, was installed at the geometric center of this slab in order to prove this assumption.
(3) Because of the symmetrical layout of the columns with respect to the longitudinal axis, the temperature of the concrete is only measured in the right column, with one thermal couple (TC35) at the center of the cross-section.
(4) The temperature at the geometric center of the right wall is measured with five thermal couples, equally distributed along the thickness of the wall.

To ensure that the thermal couples are placed at the designated locations, they were precast into concrete blocks and placed within the steel frame before concreting, see Fig. 10.

The temperature of the steel bars was measured by sensors precast into the concrete, at the depth of the concrete cover. Since the members were reinforced symmetrically, there were two values of the temperature of the steel bars for one position, namely, the temperature of the steel bars of the outer layer (referring to the steel bars distant from the surface exposed to the fire) and the temperature of the steel bars of the inner layer (meaning the steel bars close to the surface exposed to the fire). Altogether, there were 36 thermal couples: fourteen at the top slab along the middle of each span and on top of the columns and walls; fourteen at the bottom slab along the middle of each span and at the bottom of the columns and walls; two on each wall and two on each column, placed at mid-height.

3.4.2. Measurement of displacements

The displacements of the model were monitored with YHD-100 Linear Variable Differential Transformers (LVDT) throughout the

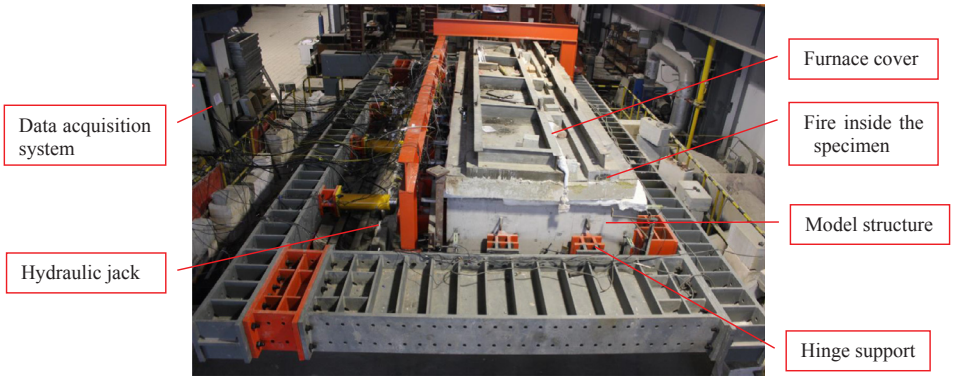

Fig. 7. Test setup of the frame in the furnace.

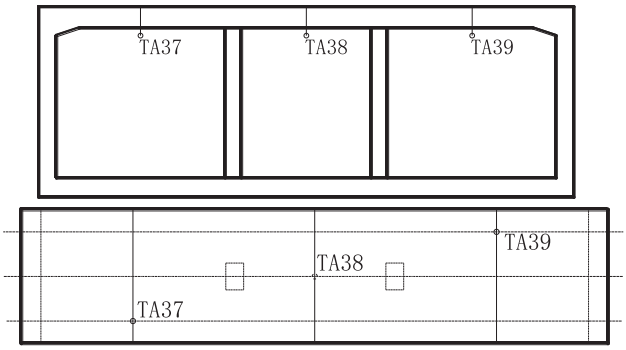

Fig. 8. Thermal couples close to the inner surface of the top slab.

testing process. The test results were automatically collected by an HP data acquisition system and recorded via a R-232 connection line. Considering the symmetry and the deformation characteristics of the model, the displacement sensors were mainly arranged at the top slab and the right wall. There were twenty-nine locations at the top slab (Fig. 11(a)), with nineteen points on the central line to measure the vertical displacement of the top slab in the width direction. Four sensors, designated as WY-F-41, WY-F-42, WY-F-43, and WY-F-44, were placed on the bottom slab, at the same positions as WY-C-1, WY-C-19, WY-C-20, and WY-C-26 on the top slab. Eleven sensors were placed on the right wall, see Fig. 11(b), and five sensors were placed on the left wall, designated as WY-LW-45, WY-LW-46, WY-LW-47, WY-LW-48, and WY-LW-49, at the same positions as WY-RW-30, WY-RW-33, WY-RW-36, WY-RW-37, and WY-RW-39 on the right wall.

To measure the relative rotations of the slabs and the walls, three precast blocks were placed in the vicinity of three corners of the structure, see Fig. 11(c). The precast blocks were assumed to be rigid, rotating together with the model. Thus, the measured rotations of the blocks represent the rotations of the slabs relative to the axis of the walls. Two LVDTs were placed at each measured corner. The difference of the measured displacements, divided by the distance between the two LVDTs, gives the rotation angle of the corner. Six LVDTs were

Fig. 10. Precast concrete blocks with thermal couples.

designated from ZJ-1 to ZJ-6, see Fig. 11(c).

In addition to the temperature, the displacements, and the rotations, all apparent phenomena including water evaporation, cracking and spalling of the concrete, and the color change of the model were recorded by cameras. After the experiment, the final depth of spalling and the width of the cracks were measured. Their locations were recorded.

4. Experimental results and discussion

4.1. Material properties

Degradation of the material properties of the used concrete, including its elastic modulus and compressive strength, were investigated. Six concrete cubes with the dimensions 150 mm × 150 mm × 300 mm were tested before the fire test. Another six samples were tested after being exposed to the fire together with the large-scale structure model. The color of the six specimens exposed to the fire turned gray, and quite a lot of pores were observed on the

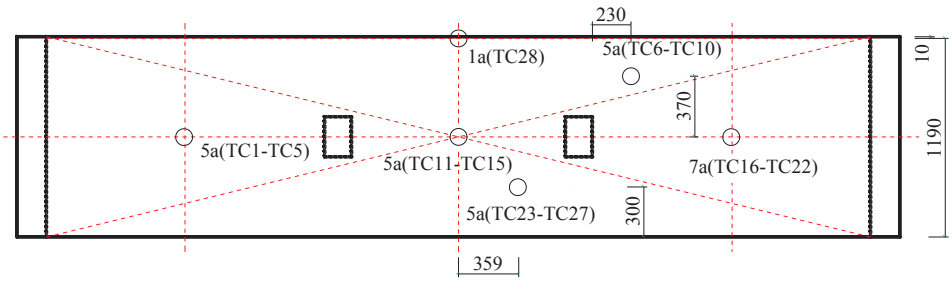

Fig. 9. Location of the thermal couples on the top slab.

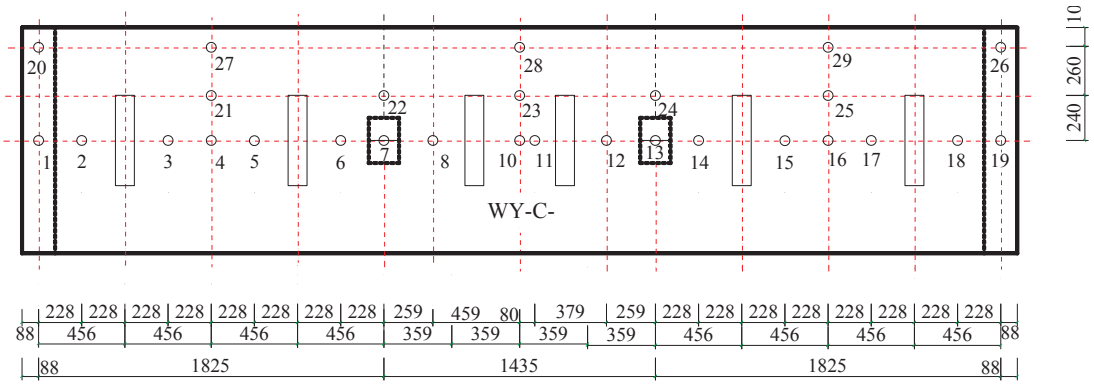

(a) displacement sensors at the top slab

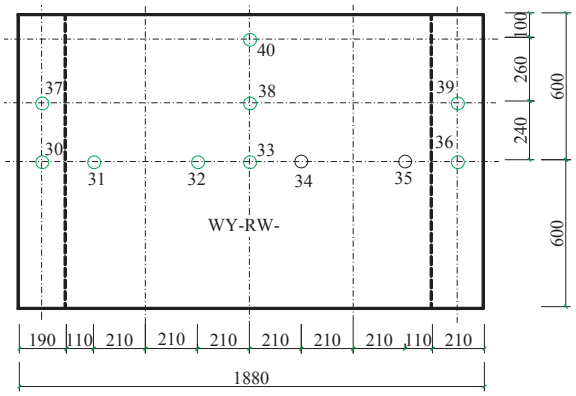

(b) displacement sensors at the right wall

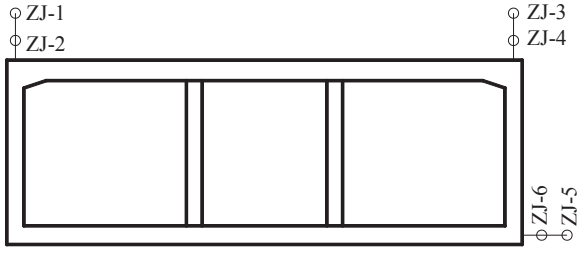

(c) displacement sensors in the vicinity of the corners

Fig. 11. Displacement sensors.

Table 5
Average material properties of concrete before and after the fire.

Concrete specimens	Properties	Before the fire	After the fire
150 mm × 150 mm × 300 mm	Elastic modulus (MPa)	2.57×10^4	1.11×10^4
	Compressive strength (MPa)	36.5	22

surface after cooling. However, no spalling of the cubes was observed.

The average decrease of the weight of the specimens after exposition to the fire was 6.51%. The elastic modulus and the compressive strength of the concrete decreased significantly, see Table 5.

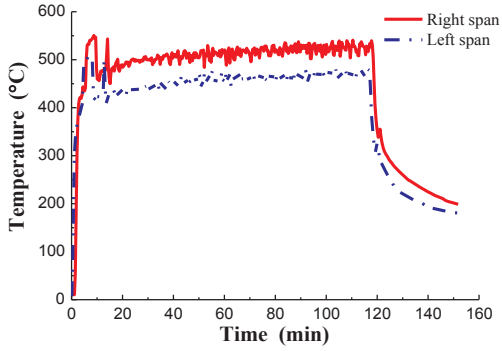

Fig. 12. Air temperature in the furnace.

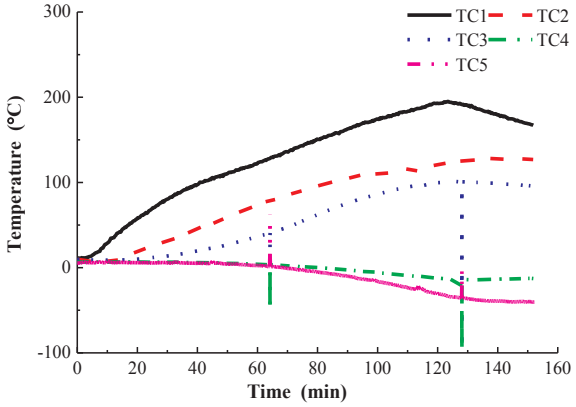

(a) 5a (TC1-TC5)

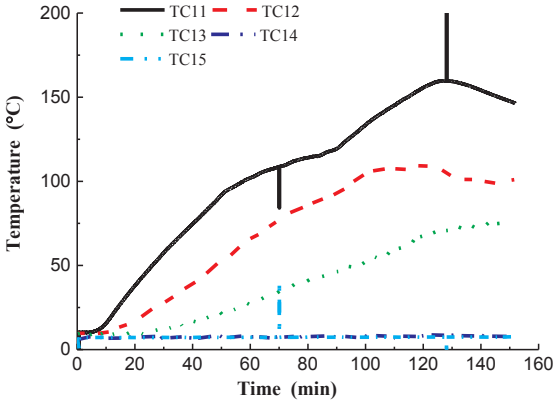

(b) 5a (TC11-TC15)

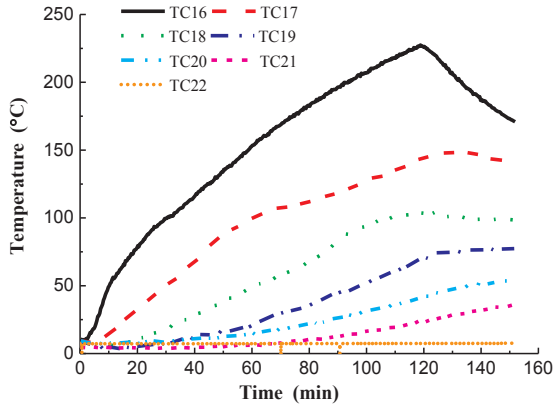

(c) 7a (TC16-TC22)

Fig. 13. Concrete temperature at different depths of the top slab (TC4, TC5, TC10, TC14, TC15 were broken).

4.2. Temperature measurement

4.2.1. Temperature of the air in the furnace

The measured evolution of the temperature of the air in the furnace is shown in Fig. 12. The measured temperature curve generally agrees quite well with the designed evolution of the temperature. The temperature of the air rises quite fast within the first ten minutes of the test, reaching around 600 °C.

The designed fire scenario was realized quite well for the right span (TA37). One of the burning nozzles on the left side turned out of work during the fire test, which resulted in an air temperature slightly lower than that on the other side (TA39). This has proved that the arrangement for placing the thermal sensors was reasonable.

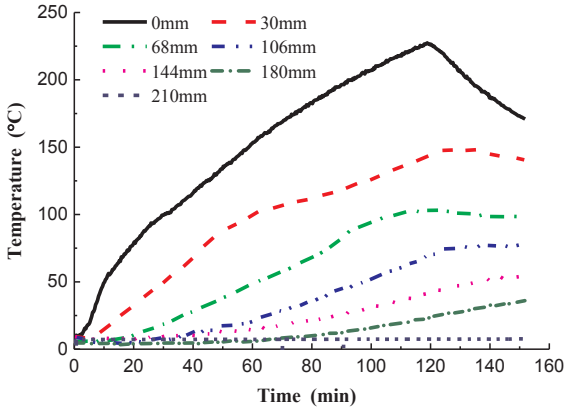

Fig. 14. Temperature along the height of the right span of the top slab.

4.2.2. Temperature of concrete

The evolution of the temperature of concrete at different depths of the right span, the middle span, and the left span of the top slab is shown in Fig. 13.

The temperature distribution along the height of the top slab and the temperature evolution at the same depth of the three spans of the top slab will be discussed in the following.

(1) Temperature distribution along the height of the top slab

The evolution of the temperature distribution along the height of the right span of the top slab is shown in Fig. 14.

(1) The temperature of the concrete first increased and then decreased. The decrease in the cooling part of the test began with a delay compared to the decrease of the temperature of the air in the furnace. Due to thermal inertia of the concrete, its temperature was still increasing for a while after termination of the heating process. This supports the conclusion that the highest temperature inside the structure is obtained after the peak of the temperature of the fire in this test.
(2) Those thermal couples, which were close to the surface exposed to the fire, recorded a fast increase of the temperature during the heating process and a fast decrease of the temperature during the cooling process. This is attributed to the large thermal gradient at these positions, leading to a fast temperature change according to the theory of thermal conduction.

(2) Temperature evolution of the three spans of the top slab

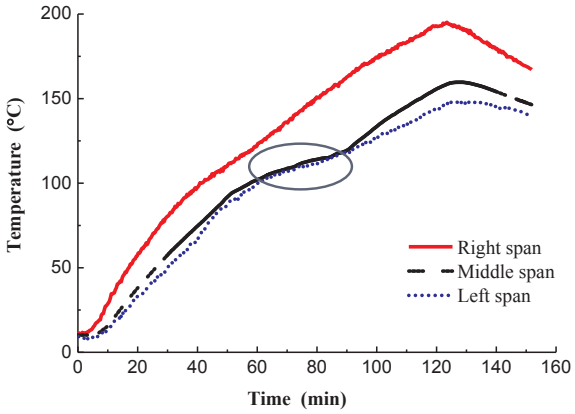

Fig. 15. Temperature evolution at the same depth (30 mm) of the three spans.

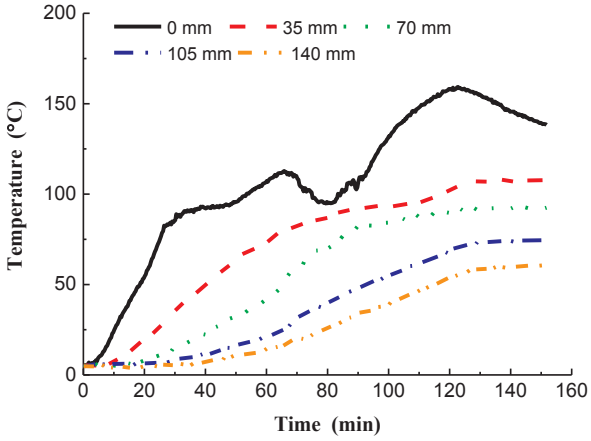

Fig. 16. Concrete temperature in the wall.

The evolution of the temperature at the left span, the middle span, and the right span of the top slab, at the same depth, i.e. 30 mm away from the fire-exposed surface, are compared in Fig. 15.

Comparing the three temperature curves, it is seen that

(1) The temperature in the right span is the highest while that in the left span is the lowest, which follows the same trend as that of the air in the furnace.
(2) There is a "plateau" of the temperature curve of the concrete at a temperature of 100–115 °C. This is the consequence of the evaporation of the water inside the material and of adsorption of the heat of concrete until all of the free water is evaporated.

The temperature evolution in the wall at depths of 0 mm, 35 mm, 70 mm, 105 mm, and 140 mm, counted from the surface exposed to the fire, is shown in Fig. 16. The temperature evolution in the geometric center of the column is shown in Fig. 17.

At the same depth, the temperature in the column increases faster than that in the walls, see Figs. 15–17, since the columns are heated from four sides. The increase of the temperature in the right column after termination of heating, i.e., after 120 mins, see Fig. 17, may be caused by spalling of the column right after the beginning of the cooling process.

4.2.3. *Temperature in the steel bars*

Fig. 18 shows the measured temperature evolution in the steel bars of the top slab, including the steel bars of the inner and the outer layers. The steel bars of the inner layer are close to the surface that is exposed to the fire. Fig. 19 refers to the measured temperature evolution in the steel bars in the right wall. Fig. 20 shows the monitored temperature

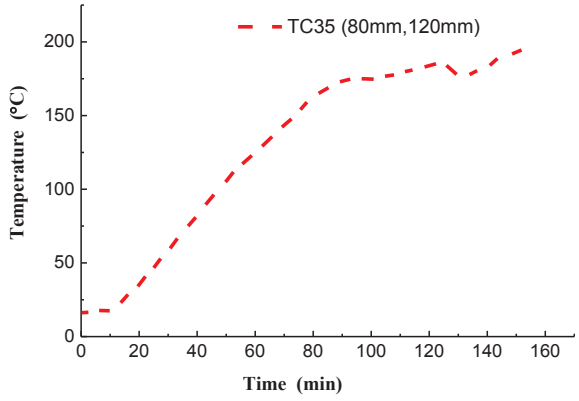

Fig. 17. Concrete temperature in the column.

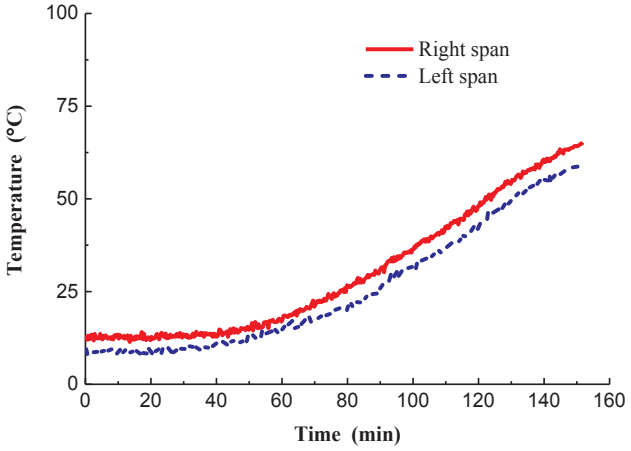

(a) inner layer steel bars

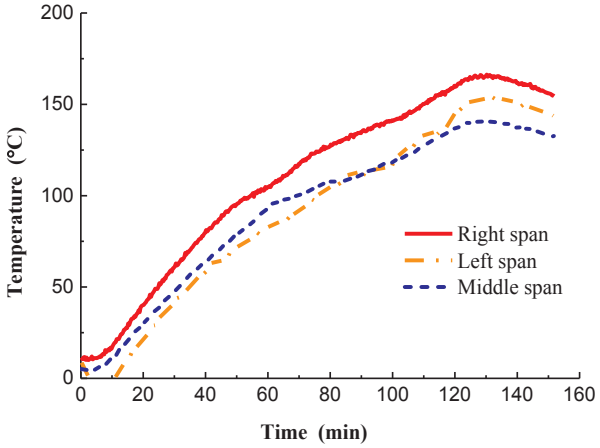

(b) outer layer steel bars

Fig. 18. Temperature evolution in the steel bars of the top slab.

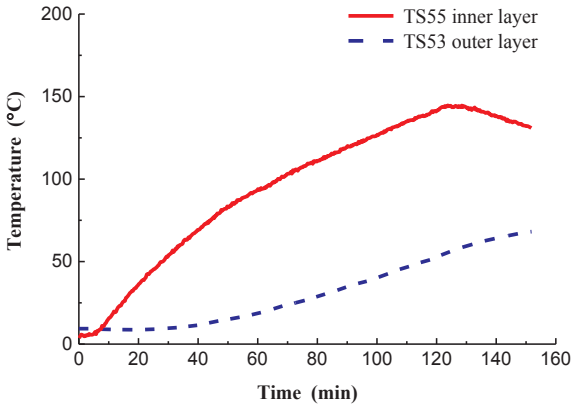

Fig. 19. Temperature evolution in the steel bars of the wall.

evolution of the steel bars in the columns.

After two hours of fire exposition, the temperature in the steel bars of the inner layer, which are close to the surface that is exposed to the fire, was nearly by 100 °C higher than that in the bars of the outer layer, see Figs. 18 and 19. The temperature of the latter shows no significant rise during the first hour. Later on, the temperature slightly increased to no higher than 100 °C. Even 30 mins after the beginning of the cooling process, the temperature in the steel bars of the outer layer was still increasing, while the temperature in the steel bars close to the fire-exposed surface exhibited only 10 mins of delay and then began to

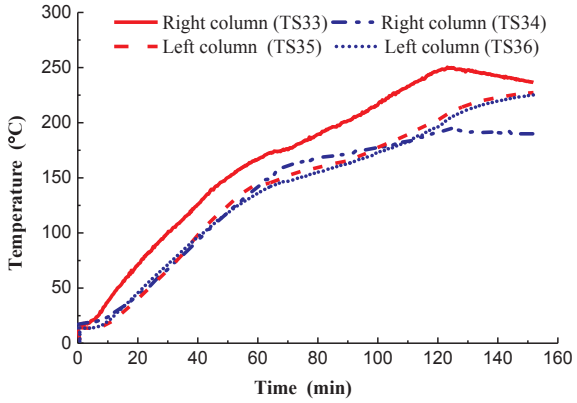

Fig. 20. Temperature evolution in the steel bars of the columns.

decrease, see Figs. 18 and 19.

During the first 90 mins of heating, the temperature of the steel bars in the right column was nearly the same as the one of the steel bars in the left column. After 90 mins, the temperature recorded by TS33 of the right column increased much faster than the temperature recorded by the other three sensors. After 120 mins of heating, it was nearly 50 °C higher than that of the left column. This can be explained by cracking of concrete before spalling.

4.3. Displacements measurements

4.3.1. Displacements of the slabs

During the loading and heating process, the whole structure experienced a rigid body motion. To account for it, the overall horizontal movement was firstly determined by means of the displacement sensors. It was subtracted from the measured results. Fig. 21 shows the displacements of the three spans of the top slab, and Fig. 22 illustrates the displacements of the right wall.

The diagrams in Figs. 21 and 22 can be interpreted as follows:

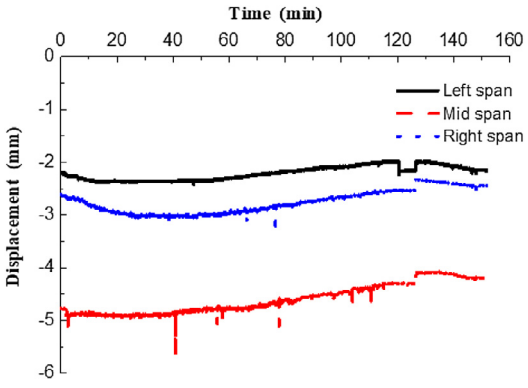

(a) mid-span displacements of the three spans of the top slab

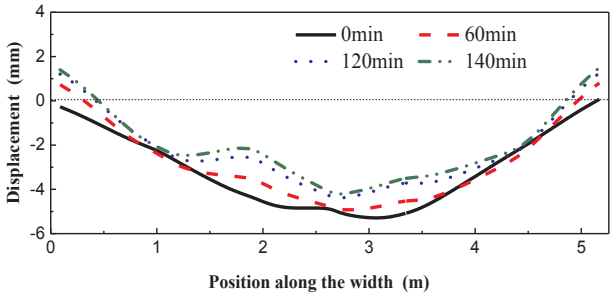

(b) displacements along the span direction of the top slab (from left to right)

Fig. 21. Displacements of the top slab.

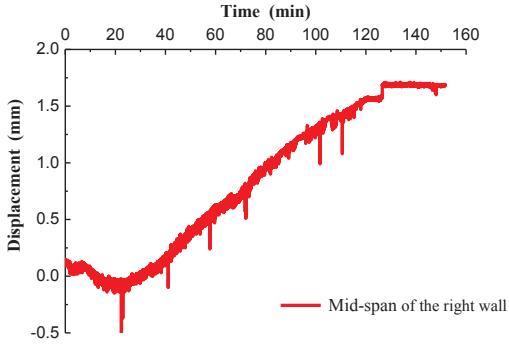

(a) mid-span displacements

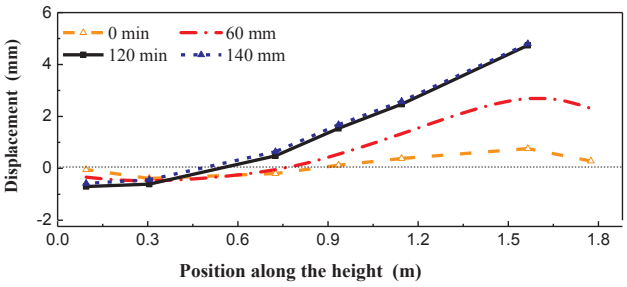

(b) displacements along the height

Fig. 22. Displacements of the right wall.

(1) In the early period of heating (0–30 mins), when the thermal expansion of the concrete is insignificant and the material properties only begin to degenerate moderately in the heating process, the mid-span displacement of all slabs tends to increase in the loading direction.
(2) In the later period of the heating (30–120 mins), the mid-span displacements of the three spans of the top slab are only slightly increasing, while that of the right wall is increasing moderately with increasing heating time.
(3) Spalling occurred 10 mins after the start of cooling. It led to a slight jump in the mid-span displacement curves for both the top slab and the right wall.

4.3.2. Rotations of the corners

The rotations of the corners were determined indirectly by means of the displacements of the two precast sensors. Fig. 23 shows the rotations of the three monitored corners, where Angle 1 and Angle 2 denote the rotations of the two corners of the top slab, while Angle 3 denotes the rotation of the right-hand corner of the bottom slab, see Fig. 11.

The diagrams in Fig. 23 can be interpreted as follows:

(1) Angle 1 shows a slight increase at the very beginning of the heating

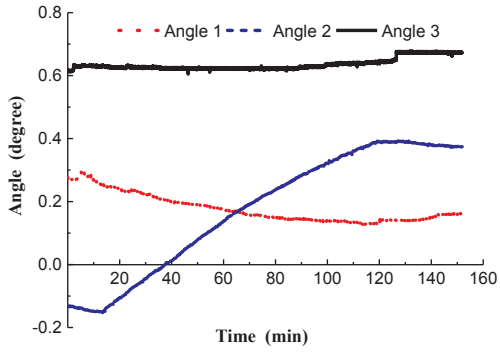

Fig. 23. Rotations of the three monitored corners.

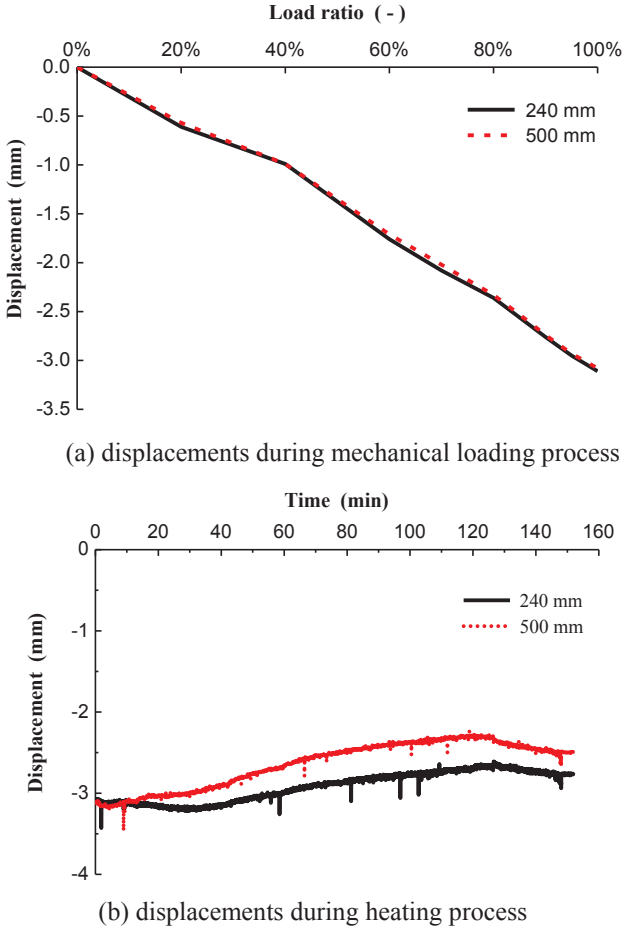

Fig. 24. Curling of the top slab.

process and then decreases with heating time due to the thermal expansion. There is a small jump when spalling of concrete occurs and a slight recovery during the cooling process.

(2) Angle 2 illustrates an increase from a negative to a positive angle after a small decrease at the beginning of the heating time. It is affected by the bending of the top slab and the thermal expansion of the right wall.

(3) Angle 3 is the rotation of the right-hand corner of the bottom slab. It does not experience a significant change during the heating process. The jump after spalling of the concrete is small.

4.3.3. Curling of the slab

Since there were no restraints on the top slab along the longitudinal direction of the station model, curling of the top slab was also expected to occur as the temperature increases. It was recorded during the fire test by comparing the measured displacements of two points at distances of 240 mm and 500 mm from the middle line in the longitudinal direction of the top slab. The displacements of these two points during the loading process are shown in Fig. 24(a), and the ones during the heating process are illustrated in Fig. 24(b). It is seen that curling did not occur during the loading process as the displacements of these two parts are almost same. However, significant curling was monitored during the heating process, indicated by the difference of the measured displacements of these two points.

4.4. Spalling and cracks

During the heating process, no spalling was detected. However, at the beginning of the cooling process, seven minutes after termination of the heating process, a loud sound of spalling was noticed. It referred to the right column. Spalling occurred at the bottom and the right surface of the right column, see Fig. 25. The concrete cover of these two parts was spalling and the inner reinforcement layers were exposed. The spalling depth was up to 60 mm. Fig. 26 shows the two largest concrete blocks found under the structure in the furnace.

(a) bottom surface of the right column

(b) right surface of the right column

Fig. 25. Spalling of the right column after the fire.

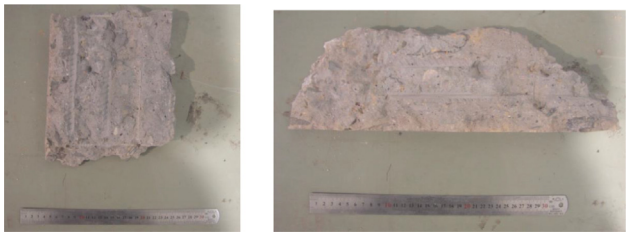

Fig. 26. Big concrete blocks found in the furnace.

Spalling did not occur at the end of the left column and in the slabs of the structure. This corroborates the conclusion that the weakest location of frame underground structures is the middle part of the columns rather than the vicinity close to its two ends.

The locations of all visible cracks were identified after the experiment and their widths were measured. Since this was done after the cooling process, most of the cracks were closed. Thus, only the distribution and the lengths of the cracks, shown in Fig. 27, are discussed herein.

Fig. 27 shows that most of the surface exposed to the fire was cracked. The cracks in the top slab were concentrated around the area connected to the columns and the walls. This suggests the conclusion that the cracks resulted from large stress concentrations caused by the restraint of thermal deformations.

(1) The columns were subjected to increased compressive loading, leading to an increase of cracking and even spalling.

(2) The non-uniform air temperature seems to be the reason for severe spalling of the column on the right side.

5. Conclusions

This paper has dealt with the description of the setup of and the results from a large-scale fire test on a substructure of a typical subway station. The test results are considered to be useful for theoretical and numerical research. The main conclusions are as follows:

(1) Due to the thermal inertia of concrete, the temperature in the concrete is still increasing for a while after termination of the

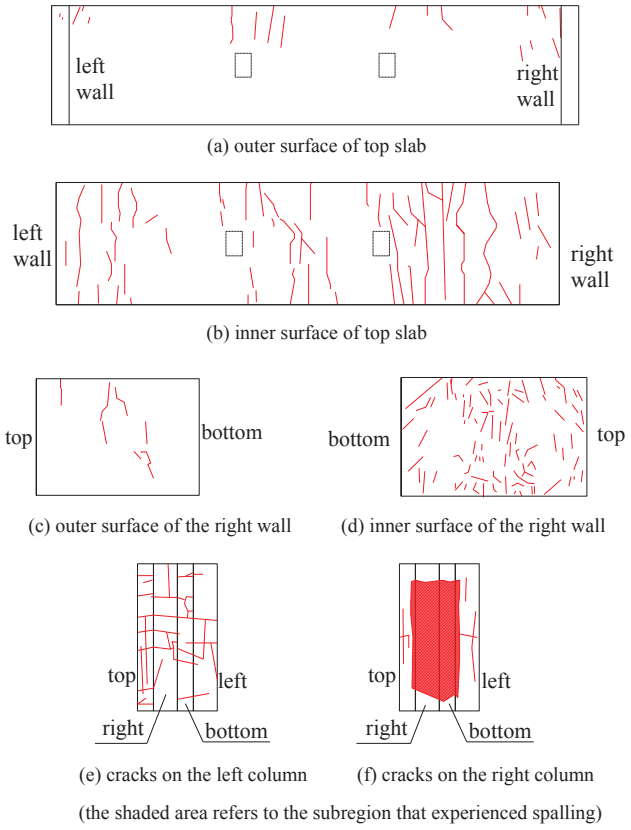

Fig. 27. Distribution of cracks in the structure.

heating process. The highest temperature inside the structure in this test occurs after termination of this process.

(2) The most seriously fire-affected members of underground structures are the columns. They are subjected to the fire at four sides and, thus, the temperature inside the column is increasing fast. Moreover, they bear a high intensity of compressive loading, which may indirectly lead to increased cracking. This suggests that the columns need more attention in fire-resistance design.

(3) During the heating process all slabs experienced a thermal expansion. While the increase of the deformations of the top slab during the heating process was relatively small, the increase of the deformations of the lateral slab during this process was significant.

(4) Since the slab does not have lateral restraints, curling occurred during the heating process.

(5) In the test, the actual fire curve was used instead of a scaled fire curve. The consequence of using the actual fire curve needs to be further studied by means of experimental tests or numerical simulations. This paper gives the results of only one large-scale fire test, more experimental tests will be necessary in the future research.

Acknowledgement

The authors wish to express their gratitude for the financial support from NSFC (No. 51208105), the Shanghai Committee of Science and Technology (16DZ1200302 & 16DZ1201904), and the Natural Science Foundation of Jiangsu Province (Grant No. BK20170282). Financial support of Hui Wang by the Austrian Science Fund (FWF), provided within the project P281 31-N32 “Bridging the Gap by Means of Multiscale Structural Analyses”, is also grateful acknowledged. The support from Dr. Lou Guobiao of SLDRCE and his colleagues is appreciated. The authors are also indebted to Mr. Cui Yanxuan and Mr. Guo Fengdi from Tongji University, and to Ms De Koning and Professor Luc Taerwe from Ghent University for their valuable help and support.

References

[1] Amouzandeh A, Moser H, Ring T, Zeiml M, Lackner R, Mang HA. Holistic analysis of underground infrastructure subjected to fire. Procedia Eng 2011;14(2259):41–51.
[2] Annerel E, Taerwe L, Jansen D, Bamonte P, Felicetti R. Thermo-mechanical analysis of an underground car park structure exposed to fire. Fire Saf J 2013;57(4):96–106.
[3] Annerel E, Lu LM, Taerwe L. Punching shear tests on flat concrete slabs exposed to fire. Fire Saf J 2013;57:83–95.
[4] Bamonte P, Felicetti R. Fire scenario and structural behaviour in underground parking garages. J Struct Fire Eng 2012;3(3):199–214.
[5] Beard A, Carvel R. The handbook of tunnel fire safety. London: Thomas Telford; 2005.
[6] British Standards Institution. Eurocode 2 (EN1992): Part 1–2 General rules – structural fire design.
[7] Heo I, Kang H, Lee DH, Oh JY, Lee JM, Kim KS. Performance-based fire behaviour analysis for underground parking structures. Int J Urban Sci 2016;20:1–11.
[8] Jiang TH, Peng JR, Zhang WM. Detection and reinforce of a reinforced concrete box culvert suffered a conflagration. Adv Mater Res 2011;228:1047–50.
[9] Lu LM, Yuan Y, Annerel E, Taerwe L. A simplified multi-iteration method for restrained beams under fire. Mater Struct 2015;48(1):9–19.
[10] Li ZL, Wu HL, Liu ZY, Xu DJ, Zhu XD. Damage assessment and repair design and implementation for underpass bridge based on fire effects. Appl Mech Mater 2012;226:1674–8.
[11] McGrattan K, Hostikka S, McDermott R, Floyd J, Weinschenk C, Overholt K. Fire dynamics simulator, User’s guide (Version 6). Nist Special Publication; 2013.
[12] McGuire JH, Stanzak WW, Law M. The scaling of fire resistance problems. Fire Technol 1975;11(3):191–205.
[13] Megret O, Vauquelin O. A model to evaluate tunnel fire characteristics. Fire Saf J 2000;34(4):282–8.
[14] O'Connor DJ, Silcock G. A strategy for the fire testing of reduced scale structural models. Fire Technol 1992;28(1):48–69.
[15] O'Connor DJ, Silcock G, Morris B. Furnace heat transfer processes applied to a strategy for the fire testing of reduced scale structural models. Fire Saf J 1996;27(1):1–22.
[16] O'Connor DJ, Morris B, Silcock G. A model fire test for parametric testing of half scale structural components. Fire Safety Sci 1997;5:997–1008.
[17] Park SH, Oh HH, Shin YS, Oh SJ. A case study on the fire damage of the underground box structures and its repair works. Tunnel Under Space Technol 2006;21(3):328. 328.
[18] Peter N. Integrated safety analysis for metro systems. In: Proceedings of the international conference on safety operation in Metro and Road Tunnels, 2011, Nov. 11–13, Shanghai, China.
[19] Ring T, Zeiml M, Lackner R. Underground structures under fire – from material modeling of concrete under combined thermal and mechanical loading to structural safety assessment. In: Proceedings of the international symposium on computational structural engineering, 2009, June 22–24, Shanghai, China.
[20] Ring T, Zeiml M, Lackner R. Underground concrete frame structures subjected to fire loading: Part I – Large-scale fire tests. Eng Struct 2014;58:175–87.
[21] Ring T, Zeiml M, Lackner R. Underground concrete frame structures subjected to fire loading: Part II – Re-analysis of large-scale fire tests. Eng Struct 2014;58:188–96.
[22] Savov K, Lackner R, Mang HA. Stability assessment of shallow tunnels subjected to fire load. Fire Saf J 2005;40(8):745–63.
[23] Standard of Test Method of Mechanical Properties on Ordinary Concrete (GB/T50081-2002). Ministry of Construction of China. Beijing, China; 2002.
[24] Standard for Metro Design (GB 50157-2003). Ministry of Construction of China. Beijing, China; 2003.
[25] Yan ZG, Zhu HH, Ju JW, Ding WQ. Full-scale fire tests of RC metro shield TBM tunnel linings. Constr Build Mater 2012;36:484–94.
[26] Yan ZG, Shen Y, Zhu HH, Li XJ, Lu Y. Experimental investigation of reinforced concrete and hybrid fibre reinforced concrete shield tunnel segments subjected to elevated temperature. Fire Saf J 2015;71:86–99.
[27] Yang Y, Cao LY. Preparatory study on scenario design for subway station. J Nat Disasters 2006;15(4):121–5.
[28] Yasuda F, Ono K, Otsuka T. Fire protection for TBM shield tunnel lining. Tunnel Undergr Space Technol 2004;19:317.
[29] Zeiml M, Amouzandeh A, Ring T, Zhang Y, Lackner R. Assessing the structural safety of underground frame structures subjected to fire loading. In: IABSE symposium report. International Association for Bridge and Structural Engineering; 2013. p. 268–273.
[30] Zhang YM, Zeiml M, Maier M, Yuan Y, Lackner R. Fast assessing spalling risk of tunnel linings under RABT fire: from a coupled thermo-hydro-chemo-mechanical model towards an estimation method. Eng Struct 2017;142:1–19.